Masarykova Univerzita
Přírodovědecká fakulta

BAKALÁŘSKÁ PRÁCE

Brno 2019 Richard Liptaj

MASARYKOVA
UNIVERZITA

Přírodovědecká fakulta
Ústav teoretické fyziky a astrofyziky

Rotační proměnnost bílých trpaslíků pozorovaných družicí KEPLER

Bakalářská práce

Richard Liptaj

Vedúci práce: prof. Mgr. Jiří Krtička, Ph.D. Brno 2019

Bibliografický záznam

Autor:	Richard Liptaj Přírodovědecká fakulta, Masarykova univerzita Ústav teoretické fyziky a astrofyziky

Název práce:	Rotační proměnnost bílých trpaslíků pozorovaných družicí KEPLER
Studijní program:	Fyzika
Obor:	Astrofyzika
Vedoucí práce:	prof. Mgr. Jiří Krtička, Ph.D.
Akademický rok:	2018/2019
Počet stran:	vii + 39
Klíčová slova:	bílí trpaslíci, rotace, fotometrická proměnnost

Bibliografic entry

Author:	Richard Liptaj Faculty of Science, Masaryk University Department of Theoretical Physics and Astrophysics
Title of Thesis:	Rotational variability of white dwarfs observed by KEPLER satellite
Degree Programme:	Physics
Field of study:	Astrophysics
Supervisor:	prof. Mgr. Jiří Krtička, Ph.D.
Academic Year:	2018/2019
Number of Pages:	vii + 39
Keywords:	white dwarfs, rotation, photometric variability

Abstrakt

Zveřejnění dat mise K2 poskytlo mnoho nových pozorování bílých trpaslíků a dovolilo nám lepší pohled na proměnnost těchto hvězd. Předložená práce spočívá na objevu a zpracování světelných křivek rotačně proměnných bílých trpaslíků. Vybrali jsme 33 bílých trpaslíků a určili jejích rotační periody. Získané výsledky jsou obecně v souladu s daty dostupnými v literatuře a s výsledky vývojových modelů.

Abstract

The data release of K2 mission provided many new observations of white dwarfs and allowed a better insight into the variability of white dwarfs. Our work consisted of discovering and processing the light curves of rotationaly variable white dwarfs. We picked 33 white dwarfs and determined their rotational periods. In general, the determined values agree with results of other papers and with products of evolutionary models.

Poďakovanie

Rád by som poďakoval svojmu vedúcemu práce profesorovi Jiřímu Krtičkovi za usmernovanie počas písania bakalárskej práci a konzultantovi profesorovi Zdeňku Mikuláškovi za výpomoc pri spracovaní dát. Taktiež by som rád poďakoval autorom článku Hermes et al. (2017) za využitie ich zoznamu bielych trpaslíkov z družice Kepler a Mikulski Archive for Space Telescopes (MAST) za poskytnutie dát.

Prohlášení

Prohlašuji, že jsem svoji bakalářskou práci vypracoval samostatně s využitím informačních zdrojů, které jsou v práci citovány.

Brno 2019

Podpis autora

MASARYKOVA UNIVERZITA
Přírodovědecká fakulta

ZADÁNÍ BAKALÁŘSKÉ PRÁCE

Akademický rok: 2018/2019

Ústav: Ústav teoretické fyziky a astrofyziky

Student: Richard Liptaj

Program: Fyzika

Obor: Astrofyzika

Ředitel *Ústavu teoretické fyziky a astrofyziky* PřF MU Vám ve smyslu Studijního a zkušebního řádu MU určuje bakalářskou práci s názvem:

Název práce: Rotační proměnnost bílých trpaslíků pozorovaných družicí KEPLER

Název práce anglicky: Rotational variability of white dwarfs observed by KEPLER satellite

Oficiální zadání:
Družice Kepler/K2 získala světelné křivky velkého množství bílých trpaslíků. Významná část pozorovaných bílých trpaslíků vykazuje rotačně modulovanou světelnou proměnnost. Příčiny této proměnnosti nejsou doposud známé. Cílem bakalářské práce je studium rotační proměnnosti bílých trpaslíků. Z archivu družice Kepler/K2 budou vybrány světelné křivky bílých trpaslíků vykazující rotační proměnnost. Pro vybrané hvězdy bude určena perioda světelných změn. V práci budou diskutovány možné příčiny proměnnosti bílých trpaslíků.

Literatura:

- Dupuis, J., Chayer, P., Vennes, S., Christian, D. J., Kruk, J. W. 2000, ApJ, 537, 977
- Hermes, J. J., Gansicke, B. T., Kawaler, S. D., et al. 2017, ApJS, 232, 2
- Krtička, J., Mikulášek, Z., Zverko, J., Žižňovský, J. 2007, A&A, 470, 1089

Jazyk závěrečné práce: angličtina

Vedoucí práce: prof. Mgr. Jiří Krtička, Ph.D.

Konzultant: prof. RNDr. Zdeněk Mikulášek, CSc.

Datum zadání práce: 28. 9. 2018

V Brně dne: 3. 4. 2019

Souhlasím se zadáním (podpis, datum):

.....	.....	.....
Richard Liptaj	prof. Mgr. Jiří Krtička, Ph.D.	prof. Rikard von Unge, Ph.D.
student	**vedoucí práce**	**ředitel Ústavu teoretické fyziky a astrofyziky**

Contents

Introduction **1**

1 White dwarfs **2**
1.1 The progenitors . . . 2
1.1.1 Low mass stars . . . 2
1.1.2 Low to medium mass stars . . . 3
1.1.3 Medium to high mass stars . . . 3
1.2 Equation of state of degenerate gas . . . 4
1.3 Mass limit . . . 5
1.4 Atmosphere . . . 6
1.5 Cooling . . . 6
1.6 Spectra . . . 7
1.7 Rotation of white dwarfs . . . 8

2 Photometric variability of white dwarfs **11**
2.1 Pulsating white dwarfs . . . 11
2.2 Companions of white dwarfs . . . 11
2.3 Surface abundance spots on white dwarfs . . . 12
2.3.1 Accretion of debris material . . . 12
2.4 Magnetic white dwarfs . . . 13

3 Kepler Space Telescope **15**
3.1 Second Light (K2) . . . 17

4 Processing of K2 data **18**

5 Conclusion **25**

Electronic references **26**

References **27**

Appendices **32**

A Light curves of white dwarfs **32**

B Atypical light curves of white dwarfs **37**

Introduction

White dwarfs are the final evolutionary state of approximately 97% stars in our Galaxy (Fontaine, Brassard, and Bergeron, 2001). The importance of studying these objects was known from the beginning. But only a small part of them shows variable magnitude. Since the first case of pulsating white dwarf (Landolt, 1968) the amount of variable white dwarfs did not increase very much.

The Kepler space observatory, which was designed to survey a part of our close neighborhood to discover Earth-size exoplants, also contributed with photometry of hundreds of white dwarfs during its operational time.

For the research of white dwarfs, K2 was the most fruitful mission. K2 started in 2014 after two of four reaction wheels failed. The mission gave us hundreds of light curves of white dwarfs that need to be analyzed to detect the light curves that show signs of variability.

Here we concentrate the light variability that can be atributed to stellar rotation.

1 White dwarfs

This chapter was written according to Mikulášek and Krtička (2005) and Murdin (2001).

Stars with mass less then 11 $M_\odot$ are destined to become a white dwarf. The mass distribution of white dwarfs is strongly peaked at 0.6 $M_\odot$, and the majority of white dwarfs have masses between $0.5M_\odot$ and $0.7M_\odot$. The estimated radii of observed white dwarfs are typically from 0.8% to 2% of the radius of the Sun; this is comparable to the Earth's radius of approximately 0.9% solar radius (Shipman, 1979). The mean density is about 10^9 kg m^{-3}, approximetly million times higher than the mean density of our Sun. A typical white dwarf has a mean density between 10^7 kg m^{-3} and 10^{10} kg m^{-3}.

Most white dwarfs do not generate energy from nuclear fusion, but radiate due to thermal energy. Because of the degenerate equation of state, contraction is accompanied by a loss of thermal energy instead of increase as in the case of ideal gases. The evolution of white dwarfs is therefore often simply described as cooling.

It takes approximately 10^{10} years for the effective temperature of a normal mass white dwarf to decrease from 100 000 K to near 5000 K. Consequently, the cool normal mass white dwarfs are still visible among the oldest objects in the Galaxy. Therefore, studying white dwarfs is extremely important to comprehend the processes of stellar formation and evolution in the Milky Way.

1.1 The progenitors

1.1.1 Low mass stars

If the mass of a main–sequence star is lower than approximately half a solar mass, it will never become hot enough to fuse helium in its core. It is thought that, over a lifespan that considerably exceeds the age of the Universe, such a star will eventually burn all its hydrogen and end its evolution as a helium white dwarf.

Due to the very long time this process takes, it is not thought to be the origin of the observed helium white dwarfs. Rather, they are thought to be the product of mass loss in binary systems or mass loss due to a large planetary companion (Laughlin, Bodenheimer, and Adams, 1997).

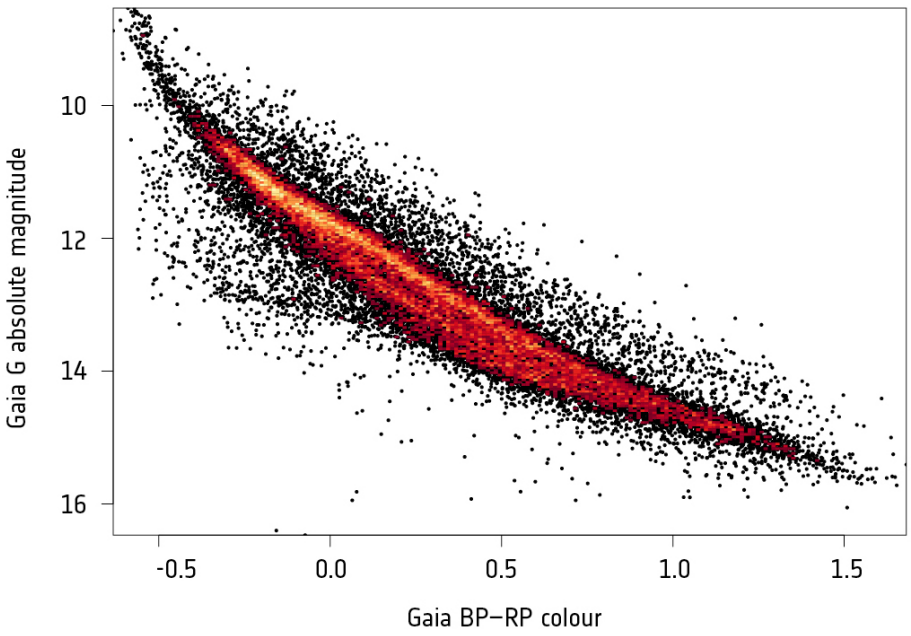

Figure 1.1: HR diagram of white dwarfs from GAIA (E1).

1.1.2 Low to medium mass stars

If the mass of a main–sequence star is between 0.5 and 8 $M_\odot$ like the mass of Sun, its core will become sufficiently hot to fuse helium into carbon and oxygen via the triple–alpha process. Near the end of the period in which it undergoes fusion reactions, such a star will have a carbon–oxygen core which does not undergo fusion reactions, surrounded by an inner helium-burning shell and an outer hydrogen-burning shell.

It will then expel most of its outer material, creating a planetary nebula, until only the carbon–oxygen core is left. This process is responsible for the carbon–oxygen white dwarfs which form the vast majority of observed white dwarfs.

1.1.3 Medium to high mass stars

If a star is massive enough, its core will eventually become sufficiently hot to fuse carbon to neon, and then to fuse neon to iron. Such a star will not become a white dwarf, because the mass of its central, non–fusing core, initially supported by the pressure gradient of electron degenerate gas, will eventually exceed the largest possible mass that can be supported by electron degenerate gas. After this the core of the star will collapse and it will explode in a core–collapse supernova which will

leave behind a remnant neutron star or black hole (Heger et al., 2003).

However, main–sequence stars of initial mass of 8 to 11 $M_\odot$, sufficiently massive to fuse carbon to neon and magnesium, may be insufficiently massive to fuse neon. Such a star may leave a remnant white dwarf composed mainly of oxygen, neon, and magnesium, provided that its core does not collapse and the fusion does not proceed so violently as to blow apart the star in a supernova (Nomoto, 1984; Woosley, Heger, and Weaver, 2002).

1.2 Equation of state of degenerate gas

This section was written according to Kvasnica (1998).

The matter of a white dwarf consists of a plasma of unbound nuclei and electrons. There is therefore no obstacle to placing nuclei closer than normally allowed by electron orbitals limited by normal matter. Since electrons obey the Pauli exclusion principle, no two electrons can occupy the same state.

The Pauli exclusion principle implies that in ideal case (at zero temperature) electrons can not all occupy the lowest–energy state; some of them have to occupy higher–energy states, forming a band of lowest–available energy states. This state of the electrons is called degenerate. The *Fermi energy*, which is the energy of the highest occupied state, is for the non–relativistic limit:

$$E_\mathrm{F} = \frac{\hbar^2}{2m_\mathrm{e}} \left(\frac{3\pi^2 N}{V} \right)^{2/3}, \tag{1.1}$$

where N is the number of particles, m the rest mass of particle and V is the volume of the system.

Despite the non–zero temperature of a white dwarf, we can still approximate the electron gas as completely degenerate gas. To find out how the degree of degeneracy depends on temperature and pressure, we can rewrite the Fermi energy as:

$$E_\mathrm{F} = \frac{\hbar^2}{2m_\mathrm{e}} \left[3\pi^2 \left(\frac{Z}{A} \right) \frac{\rho}{m_\mathrm{H}} \right]^{2/3}, \tag{1.2}$$

where Z is number of protons and A is number of nucleons in the atomic nucleus and ρ is the density.

Now we compare the Fermi energy with classical energy of an electron, which is $\frac{3}{2}kT$. If $\frac{3}{2}kT < E_\mathrm{F}$, then an average electron is unlikely to occupy free states above Fermi energy and this matter is called degenerate. After combining (1.2) with $\frac{3}{2}kT < E_\mathrm{F}$ we get:

$$T_\mathrm{D} < \frac{\hbar^2}{3m_\mathrm{e}k} \left[3\pi^2 \left(\frac{Z}{A} \right) \frac{\rho}{m_\mathrm{H}} \right]^{2/3}. \tag{1.3}$$

The expression on the right side is called the *degeneracy temperature*. Here we can see that $T_\mathrm{D} \sim \rho^{2/3}$ which means T_D grows faster than T_C where, from equation for

ideal gas, $T_{\mathrm{C}} \sim \rho^{1/3}$. This explains why every star during its evolution reaches the limit of electron degenerate gas.

The pressure can be obtained from the Grand potential Ω which is:

$$\Omega = -\frac{2}{3}E, \tag{1.4}$$

where E is the total energy of the system which equals to $3NE_{\mathrm{F}}/5$ and the required pressure of non–relativistic particles is

$$P = -\frac{\Omega}{V} = \frac{1}{5}\left(3\pi^2\right)^{2/3}\frac{\hbar^2}{m_{\mathrm{e}}}\left(\frac{N}{V}\right)^{5/3} = \frac{2}{5}\frac{N}{V}E_{\mathrm{F}}. \tag{1.5}$$

From this equation we can see that pressure of degenerate gas does not depend on temperature unlike the ideal non–degenerate gas.

1.3 Mass limit

The reletion between mass and radius of white dwarf can be derived from hydrostatic equilibrium equation:

$$\begin{gathered}\frac{P}{R} \sim G\rho\frac{M}{R^2} \;\rightarrow\; \frac{\rho^{5/3}}{R} \sim \rho\frac{M}{R^2} \;\rightarrow\; \left(\frac{M}{R^3}\right)^{2/3} \sim \frac{M}{R} \;\rightarrow \\ R \sim M^{-1/3}.\end{gathered} \tag{1.6}$$

This means that the radius of a white dwarf decreases as its mass increases. In the 20th century, Subrahmanyan Chandrasekhar found out that white dwarfs with higher mass are made of ultrarelativistic degenerate gas and the reletion (1.6) between mass and radius steepens for high–mass white dwarfs until the limiting mass called the *Chandrasekhar limit* which is approximetly 1.4 $\mathrm{M}_{\odot}$. There is no stable solution for heavier nonrotating nonmagnetic white dwarfs heavier than the Chandrasekhar limit. When reaching the Chandrasekhar limit the star collapses into a neutron star or a black hole.

Although, if the white dwarf is in a binary system with another star, the star can start to spill matter onto the white dwarf causing it to contract until it reaches the limit and explodes as a type Ia supernovae, also known as a standard candle because of its consistent peak in luminosity due to the uniform mass of white dwarfs that explode via the accretion.

However, there is a possibility that a sufficiently massive merger remnant of two white dwarfs may lead to type Ia supernovae, whose total mass exceeds the Chandrasekhar mass of white dwarfs (Webbink, 1984; Iben and Tutukov, 1984). On the contrary there have been also claims against the successes of this channel to type Ia supernovae, producing neutron stars instead (Nomoto and Kondo, 1991).

1.4 Atmosphere

Although most of white dwarfs are thought to be composed of carbon and oxygen, observations show that their emitted light comes from an atmosphere which is a residue of the star's envelope in the AGB phase and may also contain material accreted from the circumstellar medium. The envelope is believed to consist of a helium-rich layer with mass no more than 1/100 of the star's total mass, which, if the atmosphere is hydrogen-dominated, is overlain by a hydrogen-rich layer with mass approximately 1/10 000 of the stars total mass. The high surface gravity is thought to cause this by gravitationally separating the atmosphere so that heavy elements settle down.

These outer layers determine the thermal evolution of the white dwarf. The degenerate electrons inside of a white dwarf conduct heat well, therefore most of a white dwarf's mass is nearly isothermal and is kept from cooling very quickly only by its outer layers' opacity to radiation.

1.5 Cooling

The degenerate matter that makes up the bulk of a white dwarf has a very low opacity, because any absorption of a photon requires that an electron must transit to a higher empty state, which may not be possible as the energy of the photon may not be a match for the possible quantum states available to that electron, hence radiative heat transfer within a white dwarf is weak.

However, the electron degenerate matter has a high thermal conductivity. Therefore, the interior of the white dwarf maintains a nearly uniform temperature, approximately 10^7 K. An outer shell of non–degenerate matter cools from approximately 10^7 K to 10^4 K. A white dwarf remains visible for a long time because the cooling rate decreases with time.

A white dwarf will eventually, in many trillions of years, cool and become a non–radiating black dwarf in approximate thermal equilibrium with its surroundings and with the cosmic background radiation. No black dwarfs are thought to exist yet.

Although white dwarf material is initially plasma, it was theoretically predicted in the 1960s that at a late stage of cooling, it should crystallize, starting at its center. As a white dwarf core undergoes crystallization into a solid phase, latent heat is released which provides a source of thermal energy that delays its cooling.

This effect was confirmed in 2019 after the identification of a pile up in the cooling sequence of more than 15 000 white dwarfs observed with the Gaia satellite (Tremblay et al., 2019).

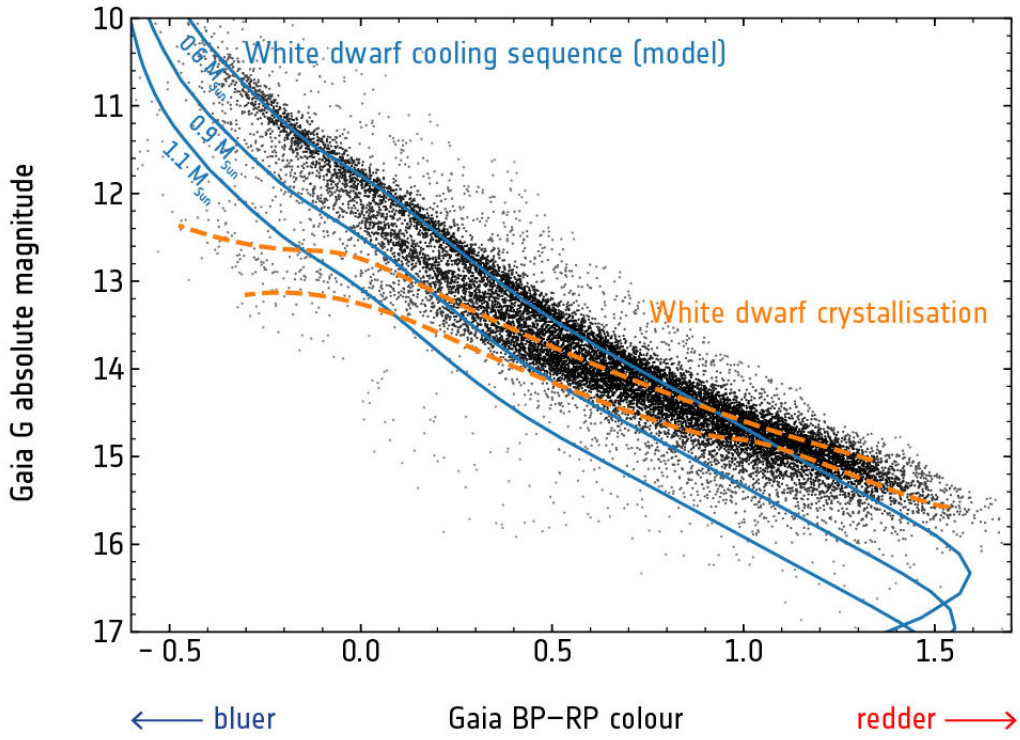

Figure 1.2: Cooling of white dwarfs with different masses and the effect of crystallizatio (E2).

1.6 Spectra

The characteristic sign of white dwarf's spectra is strong broadening of lines due to high density in atmospheres. The spectra show redshift caused by energy loss of photons forced to get through strong gravity of white dwarf. This can be used to determine white dwarf mass in a big sample of white dwarfs.

White dwarfs are classified by a symbol which consists of an initial D, a letter describing the primary feature of the spectrum followed by an optional sequence of letters describing secondary features of the spectrum.

The majority, approximately 80%, of all observed white dwarfs consists of DA white dwarfs which have hydrogen-dominated atmospheres. Their spectra show only hydrogen absorption lines broadened by pressure.

DB white dwarfs constitute the second class of white dwarfs, which makes about 16% of all white dwarfs, with atmospheres made only from helium and therefore they show helium absorption lines in their spectra.

DC is another class of white dwarfs with continuous spectrum, DO are white dwarfs with He II lines, accompanied by He I or H lines and DQ are white dwarfs that have carbon–dominated atmospheres (Kepler et al., 2007).

Approximately 25% to 33% of white dwarfs have metal lines in their spectra and these white dwarfs are called DZ. It's unusual because the heavy elements should sink into the white dwarf in a small amount of time compared to its lifetime. The prevailing explanation for metal–rich white dwarfs is that they have recently accreted rocky planetesimals (Jura and Young, 2014).

1.7 Rotation of white dwarfs

Hermes et al. (2017) were able to use their spectroscopic observations to constrain, for the first time in a systematic way, white dwarf rotation as a function of mass. They found that white dwarfs with masses between $0.51 - 0.74\,\mathrm{M}_\odot$ (within 1σ of the field white dwarf mass distribution) have a mean rotation period of 35 hr and a standard deviation of 28 hr. Using cluster–calibrated initial–to–final mass relations, such white dwarfs evolved from $1.7 - 3.0\,\mathrm{M}_\odot$ ZAMS progenitors. Therefore, they are putting narrowing boundary conditions on the endpoints of angular momentum evolution in the range of masses probed deeply by the Kepler spacecraft in earlier stages of stellar evolution. Given the slow rotation of apparently isolated white dwarfs, it thus appears from Kepler that most internal angular momentum is lost on the first–ascent giant branch.

García-Segura et al. (2014) calculated the initial total angular momentum of the $2.5\,\mathrm{M}_\odot$ star $J_{\mathrm{ZAMS}} = 7.095 \times 10^{50}\,\mathrm{g\,cm^2\,s^{-1}}$. At the end of the AGB, when $t = 7.80637 \times 10^8\,\mathrm{yr}$, the values for the radius and rotational velocity are $R = 463\,\mathrm{R}_\odot$ and $v_{\mathrm{surf}} = 296\,\mathrm{cm\,s^{-1}}$. That time represents the moment the star reaches the largest radius, just before the last thermal pulse, and when the mass–loss rate is the largest for a longer period of time. Integrating the stellar structure, they then obtained a total angular momentum of $J_{\mathrm{AGB}} = 5.667 \times 10^{48}\,\mathrm{g\,cm^2\,s^{-1}}$. The decrease of two orders of magnitude, i.e., a factor of 125, is due to mass loss (Heger and Langer, 1998). This angular momentum can be split in $J_{\mathrm{core}} = 4.0181 \times 10^{48}\,\mathrm{g\,cm^2\,s^{-1}}$ and $J_{\mathrm{env}} = 1.649 \times 10^{48}\,\mathrm{g\,cm^2\,s^{-1}}$, for the core and the envelope, respectively, where the CO core has a mass of $M_{\mathrm{core}} = 0.656\,\mathrm{M}_\odot$ and the envelope $M_{\mathrm{env}} = 0.352\,\mathrm{M}_\odot$, and a total mass $M_{\mathrm{tot}} = 1.008\,\mathrm{M}_\odot$.

Suijs et al. (2008) showed in their paper that angular momentum transport through rotationally-induced magnetic fields, according to Spruit (2002), provides a major improvement of the predicted spins of white dwarfs and neutron stars. Magnetic angular momentum transport also appears the most promising candidate to bridge the still existing gap between observed and predicted white dwarf spins at

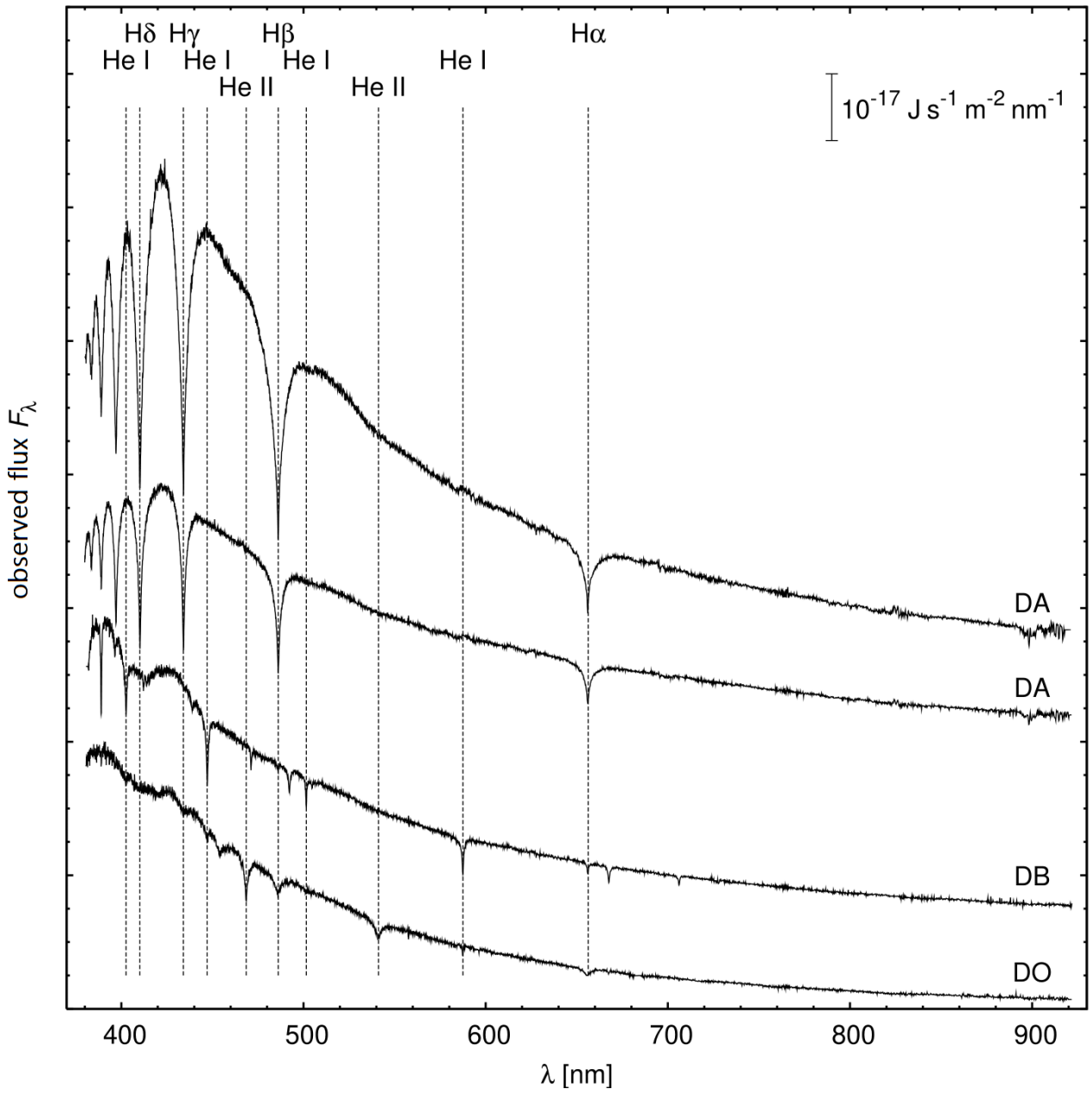

Figure 1.3: Spectra of different white dwarf classes [taken from Mikulášek and Krtička (2015) and edited].

low mass. If internal magnetic torques in their progenitors are indeed resopnsible for the slow rotation of compact stars in the Milky Way, then there may be little room for an important role of angular momentum in their formation process, at least in single stars.

However magnetic torques may not be the only mechanism to provide a spin–down of the stellar core. For example, Charbonnel and Talon (2005) invoked angular momentum transport though gravity waves (Zahn et al. 1997) to explain the slow rotation of the Solar core (Suijs et al., 2008).

2 Photometric variability of white dwarfs

A photometric variability means that a star varies in its luminosity as seen from Earth. We distinguish between two categories of variable stars: intrinsic or extrinsic. It depends on the cause of the variability.

Intrinsic variability means that the star is variable due to physical changes in the star itself and extrinsic variability happens because of eclipses or the star's rotation. Here we discuss several types of photometric variability of white dwarfs.

The magnitude of white dwarfs range from 10 mag to 17 mag (Luyten, 1949). Changes in the magnitude of discovered rotationaly variable white dwarfs in this work cover a wide range – from thousandths of a magnitude in amplitude to a tenth of a magnitude as shown in Table 4.1.

2.1 Pulsating white dwarfs

HL Tau 76 was the first variable white dwarf found and it was observed to vary with a period of approximately 12.5 minutes (Landolt, 1968). However the period was longer than predicted and the reason for this is that the variability of HL Tau 76 arises from non–radial gravity wave pulsations (Koester and Chanmugam, 1990).

Generally, pulsating white dwarfs are multimode pulsators, which exhibit more than just a single period. In some cases, the pulsation spectrum contains linear frequency combinations of genuine pulsation eigenmodes, likely produced by the outer convection zone of the star (Murdin, 2001).

The known types of pulsating white dwarfs are DAV and ZZ Ceti stars, which are DA spectral type variables; DBV and V777 Her stars, variables with DB spectral type and GW Vir stars with atmospheres mostly of helium, carbon and oxygen. These variables exhibit variations of 1% – 30% in light, arising from a superposition of vibrational modes with periods of hundreds to thousands of seconds (Murdin, 2001).

2.2 Companions of white dwarfs

One of the reasons for variable changes in white dwarfs observations could possibly be explained by the effects of companions – e.g. beaming (Zucker, Mazeh, and

Alexander, 2007) due to motion caused by a compact companion (although such close double degenerates are rare (Maoz and Hallakoun, 2017; Maoz, Hallakoun, and Badenes, 2018)), or reflection/reradiation by a heated giant planet (no planets around white dwarfs have yet been discovered (Fulton et al., 2014)) or a brown dwarf companion (although no more than approximately 2 per cent of white dwarfs have brown dwarf companions (Gänsicke et al., 2011; Barstow et al., 2011)).

2.3 Surface abundance spots on white dwarfs

The cause for the variability of main–sequence chemically peculiar stars lies in surface abundance spots where the flux redistribution due to bound–bound and bound–free transitions is modulated by stellar rotation leading to light variability (Krtička et al., 2018).

Krtička et al. (2018) discussed that white dwarfs may also have surface abundance spots either owing to the elemental diffusion or as a result of accretion of debris material around the star. They assumed that the abundance anomalies in main–sequence chemically peculiar stars caused by the radiative diffusion can be important in hot white dwarfs. Moreover, the accrection of debris material is also probably connected with surface abundance spots in white dwarfs.

Their calculations of the light curves for a warm white dwarf assumed a spot with a solar abundance of heavy elements with the surface made only of pure hydrogen. Spot like this can cause photometric variability with amplitude about a few 0.01 mag, decreasing with increasing wavelength.

2.3.1 Accretion of debris material

Studies have shown that many white dwarfs accrete the debris of their former planetary systems (Jura, 2003; Zuckerman et al., 2003; Zuckerman et al., 2010). White dwarf debris accretion is sometimes evidenced in the discs detected around some white dwarfs within the tidal disruption radius for typical asteroid densities. The discs appear as infrared–excess dust emission (Kilic et al., 2006), or as optical emission lines from gas (Manser et al., 2015).

However, the most frequent manifestation of debris accretion is the presence of the photospheric ultraviolet (UV) metal absorption lines (typically Si, but sometimes C and other elements). The sinking timescales in the strong surface gravity of most white dwarfs are relatively short. In hydrogen–dominated atmosphere (DA) white dwarfs with effective temperatures between 12 000 K and 25 000 K, heavy elements would disappear from the white dwarf atmosphere within weeks or less (Koester and Wilken, 2006; Koester, 2009).

Thus, the presence of the metal lines indicates ongoing accretion of rocky material in at least 30 per cent of all white dwarfs (Koester, Gänsicke, and Farihi, 2014).

2.4 Magnetic white dwarfs

Magnetic white dwarfs are stellar remnants featuring global magnetic structures with field strengths from 1 kG to 1 000 MG. They account for a significant part of the white dwarf population with an estimated fraction from 10% to 20% in volume complete samples (Liebert, Bergeron, and Holberg, 2003; Schmidt et al., 2003; Kawka et al., 2007). Most of these objects are high–field magnetic white dwarfs (HFMWD), with field strengths B > 1 MG, and a distribution of magnetic field strengths that appears to peak around 20 MG (Schmidt et al., 2003; Külebi et al., 2009).

Magnetic fields in white dwarfs have often been assumed to be fossil fields with the progenitors of magnetic white dwarfs being predominantly magnetic Ap and Bp stars. Assuming magnetic flux conservation, the field strengths observed in Ap/Bp stars would correspond to white dwarf fields in excess of 10 MG (Kawka and Vennes, 2004; Wickramasinghe and Ferrario, 2005). Therefore, the progenitors of white dwarfs with weak magnetic fields may be other main–sequence stars that have magnetic fields well below current detection limits (Kawka, 2018).

Tout et al. (2008) proposed a binary origin where the magnetic field is formed via a dynamo created during a common envelope (CE) phase. In systems that merge during the CE phase, single magnetic white dwarfs are created, but failed mergers would result in binary systems with a secondary nearly filling its Roche lobe. Following up on this theory, Potter and Tout (2010) and Wickramasinghe, Tout, and Ferrario (2013) showed that a magnetic field can be generated by a dynamo created by differential rotation within the CE, with the strongest fields being created if the merged objects are differentially rotating near break–up.

A variation on the merger scenario was proposed by Nordhaus et al. (2011) who proposed that during a CE phase a low–mass star will be tidally disrupted by its proto–white dwarf companion forming an accretion disk. This would generate a dynamo in the disk which is then transferred to the degenerate core via accretion. Magnetic fields can also be produced by the merger of two white dwarfs. García-Berro et al. (2012) have shown that the merger of two white dwarfs can generate a hot, convective and differentially rotating corona producing a dynamo and the resulting magnetic field.

Isern et al. (2017) proposed that magnetic fields with $B \lesssim 0.1$ MG may be produced by phase separation during the onset of crystallization in the white dwarf core. They show that as white dwarfs begin to crystallize at sufficiently low temperatures ($\sim$ 8000 K), phase separation of the main elements (in most cases O and C) occurs leading to an unstable, convective liquid mantle on top of a solid core. This produces a dynamo allowing the creation of a magnetic field.

Briggs et al. (2015) conducted a population synthesis of binary systems to investigate which type of system could result in a magnetic white dwarf. They found that the contribution from the double degenerate merger scenario is much smaller than the contribution from the CE merger. Both merger scenarios are able to explain the

higher than average mass of magnetic white dwarfs. Once the field is established, the predicted magnetic field strengths should remain throughout the white dwarf life–time since the magnetic flux is not expected to decay significantly once the magnetic field is frozen into the white dwarf (Kawka, 2018).

Tremblay et al. (2015) demonstrated that the partial or total suppression of convection is unable to change the average surface temperature until there is coupling between the convection zone and the degenerate core at low $T_{\rm eff}$ values. They noted that if the magnetic field is moving at the surface, the envelope would take some time to adjust to the new surface conditions.

The Kelvin–Helmholtz timescale of the portion of the envelope including the entire convection zone is one estimate for this thermal relaxation time, which varies from about one second at 12 000 K to about 1000 yr at 6000 K.

However, photometric variations are observed in hot magnetic white dwarfs where no convection is predicted, hence it is already clear that convective effects are not involved in some cases. Explanations for photometric variations of these stars are magneto-optical effects involving radiative transfer under different polarizations (Martin and Wickramasinghe, 1979; Martin and Wickramasinghe, 1986; Christian et al., 1997).

3 Kepler Space Telescope

The Kepler spacecraft launched in March 2009 and spent a little over four years monitoring more than 150 000 stars in the Cygnus–Lyra region with continuous 30–min or 1–min sampling. The primary science objective of the Kepler mission was transit–driven exoplanet detection with an emphasis on terrestrial ($R < 2.5R_{Earth}$) planets located within the habitable zones of Sun–like stars (E3).

Kepler is in an Earth–trailing heliocentric orbit, which insured a thermally stable environment and provided the ability to remain on a single pointing for the duration of the prime Kepler mission. Quarterly rolls were performed – one roll every 93 days – to reorient the solar arrays. With each roll, the stars in the field of view landed on different regions of the detector relative to their pre–roll position, introducing quarterly discontinuities in the light curve (E4).

The Kepler spacecraft hosts 0.95–m aperture Schmidt telescope. The primary instrument aboard Kepler is the focal plane array consisting of 21 science and 4 Fine Guidance Sensor CCD modules. Field flattener lenses on each module map the spherical telescope image surface onto the flat CCD chips, and define the overall wavelength bandpass. Each science module is an array of 2200×2048 pixels. These 21 modules each have 4 output channels, for a total of 84 channels and 94.6 million active pixels that view the sky, with additional masked real pixels and virtual pixels for collection of collateral data. As of July 2018, three of the modules were no longer in working order. The Kepler photometer utilizes one broad bandpass, ranging from 420 to 900 nm The shape of the bandpass, in Figure 3.2, was chosen to contain most of the optical spectrum (E4).

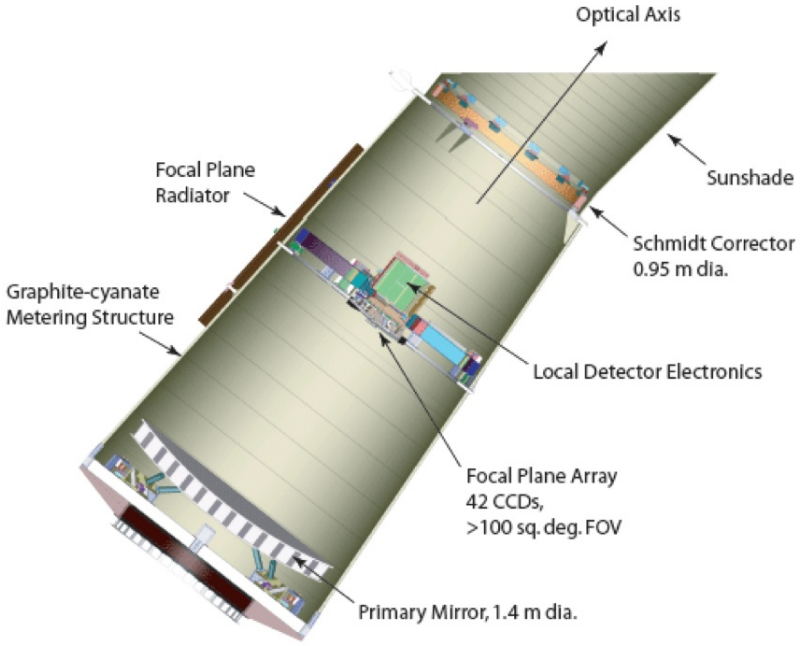

Figure 3.1: The Kepler focal plane detectors and the optical elements within the Kepler telescope (E4).

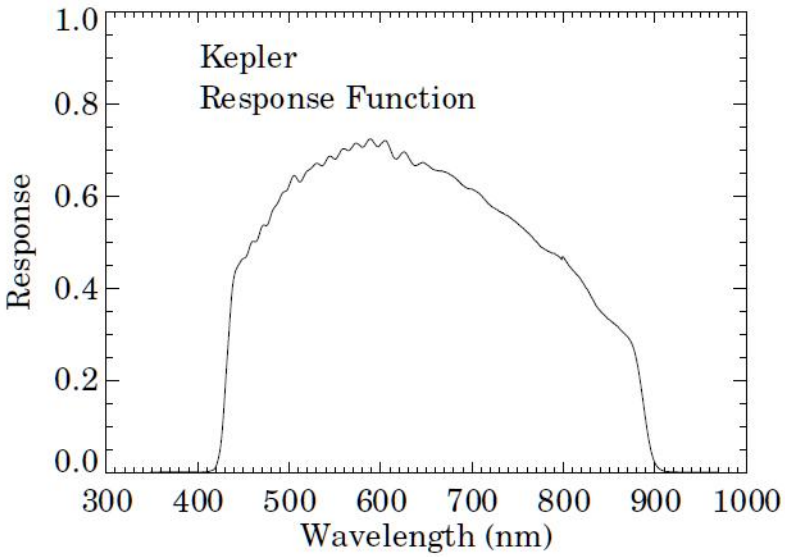

Figure 3.2: This response curve was derived during pre-flight testing and represents the laboratory calibration of the Kepler photometer (E4).

3.1 Second Light (K2)

After the loss of a second of the four reaction wheels on board the Kepler spacecraft in May 2013, the K2 mission represented a new concept for spacecraft operations that enabled continued scientific observations with the Kepler space telescope. K2 became fully operational in May 2014 and continued operating until October 2018 when Kepler ran out of fuel (E5).

Using the transit method to detect brightness changes, the K2 mission entailed a series of sequential observing "Campaigns" of fields distributed around the ecliptic plane and offered a photometric precision approaching that of the original Kepler mission. Operating in the ecliptic plane minimized the torque exerted on the spacecraft by solar wind pressure, reducing pointing drift to the point where spacecraft attitude could effectively be controlled through a combination of thrusters and the two remaining reaction wheels. Each campaign was therefore limited by sun angle constraints to a duration of approximately 80 days (E5).

The K2 mission observed 100 square degrees for 80 days each across 20 different pointings along the ecliptic. While the mission continued to observe stars to detect transiting exoplanets, the variety of pointings enabled a wider variety of astrophysical research projects; in fact the K2 mission was fully Guest Investigator-driven. The mission produced the same pixel-level and lightcurve data products as the original Kepler mission, however, the mission's planet search pipeline was not run (E6).

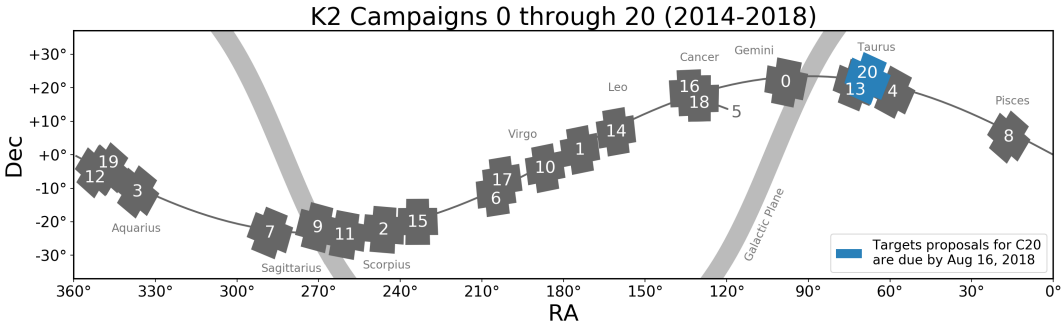

Figure 3.3: Map of Observations (E6).

4 Processing of K2 data

We used a list of more than 1600 high-probability and spectroscopically confirmed white dwarfs observed by Kepler through K2 Campaign 15 from Hermes et al. (2017) paper (E7). All the data of the light curves of white dwarfs were obtained from Mikulski Archive for Space Telescopes (MAST) where the data is publicly available (E8). We downloaded it from a ftp server after sending an email containing the IDs of all white dwarfs we wanted to retrieve and investigate.

When we had all the light curves required for our work we searched for the signs of the periodic changes in each one of the light curves of the white dwarfs on the list. From the first look we narrowed it down from an amount of about 1600 white dwarfs to approximately 70 white dwarfs which showed signs of variability to us. Then we visually inspected the light curves again and ruled out the light curves that showed synthetic periodic changes likely made by the instrumental efects of the Kepler Space Telescope after which we were left with approximately 45 white dwarfs.

Afterwards we used a program called periodogram (Mikulášek, private communication) to find out the period and the amplitude of the changes in the magnitude of the remaining white dwarfs and to take out another set of white dwarfs that did not show variability that can be atributed to rotation. We took PDCSAP_FLUX and TIME columns from the long–cadence data of K2 mission and used our periodogram to calculate the difference between apparent magnitude and the mean of the apparent magnitude $\widetilde{m}$ from the flux and to convert the time into the phase, which were calculated from Pogson equation:

$$\Delta m = -2.5\log_{10}(\text{PDCSAP\_FLUX}) - \widetilde{m}, \tag{4.1}$$

Then we used a cycle of our range of frequencies that calculated a matrix of sine and cosine functions of given frequencies and time,

$$X = \begin{pmatrix} \cos(2\pi t f) & \sin(2\pi t f) \\ \vdots & \vdots \end{pmatrix}, \tag{4.2}$$

where t is TIME, f is a frequency from our range and applied it to compute the amplitude of the frequency of the changes as

$$\sqrt{8(u^{\mathrm{T}}/v)\cdot u/N}, \tag{4.3}$$

where $u = X^{\mathrm{T}} \cdot \Delta m$, $v = X^{\mathrm{T}} \cdot X$ and N is the number of measurements. The period was calculated as a reciprocal for the maximum amplitude (Mikulášek and Zejda, 2013). At first we used a simple program to remove outliners with the biggest spread that helped us to fit with better accuracy. We fitted the data of the light curves with a harmonic fit of a second order:

$$\begin{aligned} f = A_1 \cos(2\pi\phi) + A_2 \sin(2\pi\phi) + A_3 \cos(4\pi\phi) \\ + A_4 \sin(4\pi\phi) + A_5 \end{aligned} \tag{4.4}$$

and a third

$$\begin{aligned} f = A_1 \cos(2\pi\phi) + A_2 \sin(2\pi\phi) + A_3 \cos(4\pi\phi) + A_4 \sin(4\pi\phi) \\ + A_5 \cos(6\pi\phi) + A_6 sin(6\pi\phi) + A_7 \end{aligned} \tag{4.5}$$

or a fifth order

$$\begin{aligned} f = A_1 \cos(2\pi\phi) + A_2 \sin(2\pi\phi) + A_3 \cos(4\pi\phi) + A_4 \sin(4\pi\phi) \\ + A_5 \cos(6\pi\phi) + A_6 \sin(6\pi\phi) + A_7 \cos(8\pi\phi) + A_8 \sin(8\pi\phi) \\ + A_9 \cos(10\pi\phi) + A_{10} \sin(10\pi\phi) + A_{11} \end{aligned} \tag{4.6}$$

where ϕ is the phase and $A_1 - A_{11}$ were determined as

$$A = F \backslash Y, \tag{4.7}$$

where Y are the values of Δm,represnted as a N×1 matrix, and F is

$$F = \begin{pmatrix} \cos(2\pi\phi) & \sin(2\pi\phi) & \cos(4\pi\phi) & \sin(4\pi\phi) & \dots & 1 \\ \vdots & \vdots & \vdots & \vdots & \vdots & \vdots \end{pmatrix}. \tag{4.8}$$

However we wanted to suppress outliners that had smaller deviation so we assigned every point with a weight according to their difference from the mean value of their magnitude. The weight was determined as

$$w = 1.05 e^{-\left(\frac{\Delta Y}{4s}\right)^4}, \tag{4.9}$$

where s is the standard deviation.

In Figure 4.1 we can see that the spread of the outliners is uniform over the whole light curve therefore our weighted and unweighted fits do not differ significantly. For that reason we decided not to use the wieghted fits since it makes very subtle difference.

The processing of the light curves was made in GNU Octave, version 4.2.2 with few Matlab scripts and in Python 3.

Table 4.1: Calculated periods and amplitudes of discovered rotationaly variable white dwarfs

K2 ID	Period [d]	Amplitude [mag]	K2 ID	Period [d]	Amplitude [mag]
201287505	16.502	0.029	220171396	0.4720	0.068
201292141	0.8437	0.059	220178204	1.0982	0.018
201391671	0.4135	0.025	220512358	4.0917	0.119
201475790	0.3886	0.013	220697132	3.0931	0.005
201540753	11.074	0.008	228682372	0.4776	0.051
206093851	15.528	0.007	228682397	8.6505	0.004
206197016	0.8291	0.075	246032223	13.643	0.020
206293521	13.495	0.017	248460642	2.3079	0.011
210609259*	2.0404	0.037	248473806	3.2520	0.005
211375959	4.5956	0.025	248563865	1.5031	0.039
211434324	1.6308	0.022	248596522[a]	2.1659	0.038
211481191*	2.6240	0.061	248744651	1.0765	0.017
211719633	5.4885	0.011	248750313	25.189	0.002
211815847	4.5977	0.043	248774401	0.8645	0.004
211949591	12.594	0.024	249660366	2.6846	0.028
211995459*	2.2232	0.052	250152017	5.0025	0.005
220155299	5.5648	0.013			

a - WD 248596522 shows variable amplitude. * - WDs showing secondary minimum (210609259 - 0.014 mag, 211481191 - 0.018 mag, 211995459 - 0.038 mag).

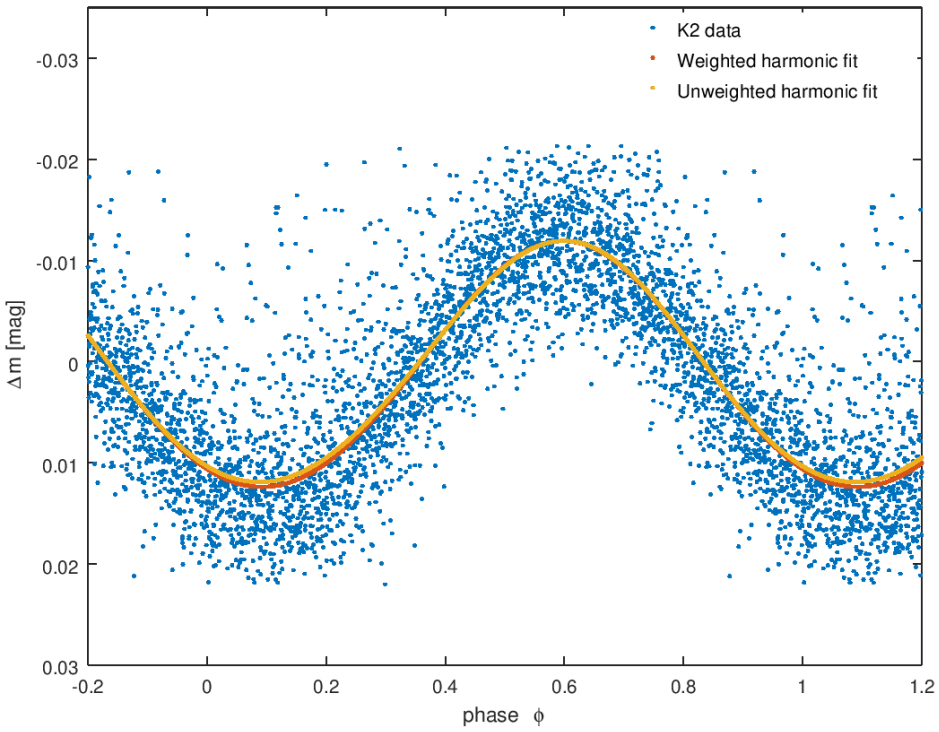

Figure 4.1: Comparison of weighted and unweighted fit ofthe light curve of the white dwarf EPIC 201391671

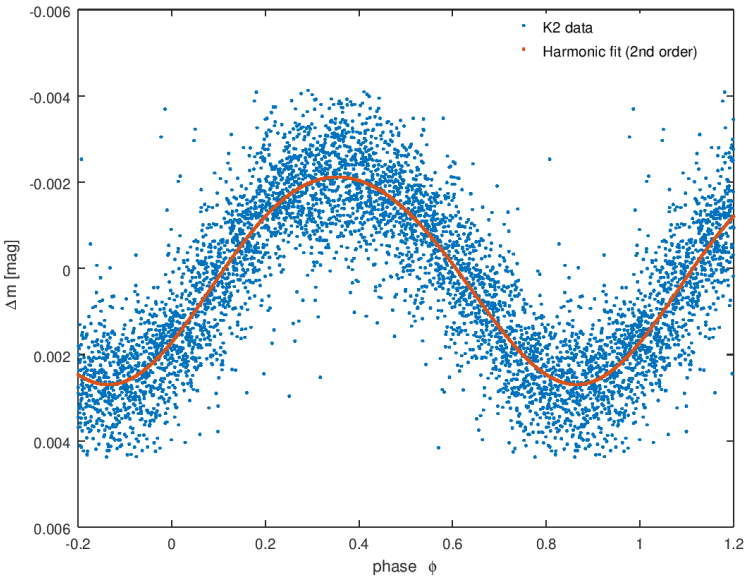

Figure 4.2: Comparison of observed and fitted data of white dwarf with EPIC 250152017.

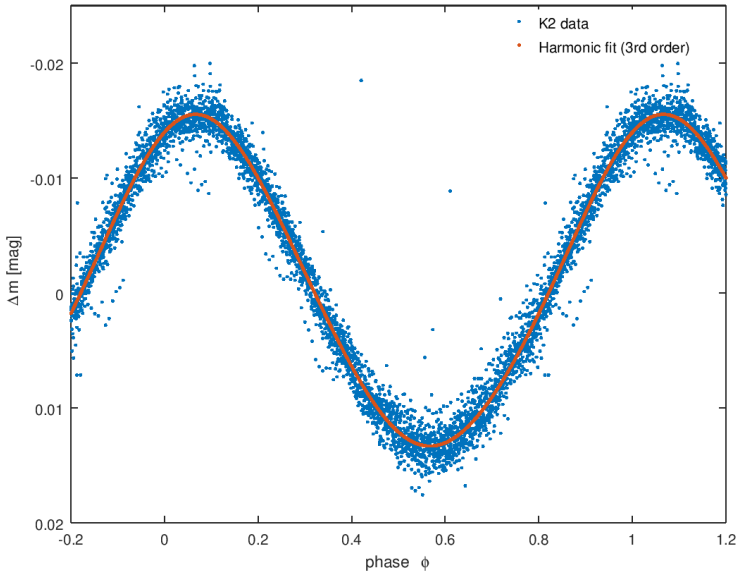

Figure 4.3: Comparison of observed and fitted data of white dwarf with EPIC 249660366.

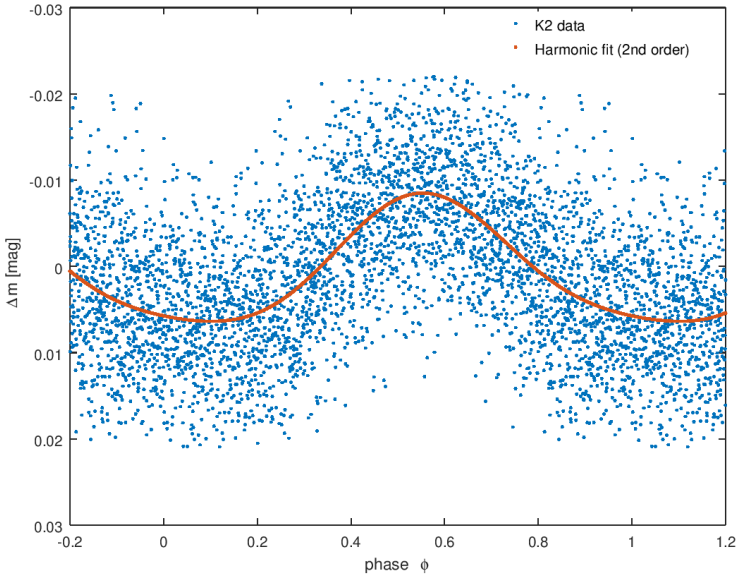

Figure 4.4: Comparison of observed and fitted data of white dwarf with EPIC 248744651.

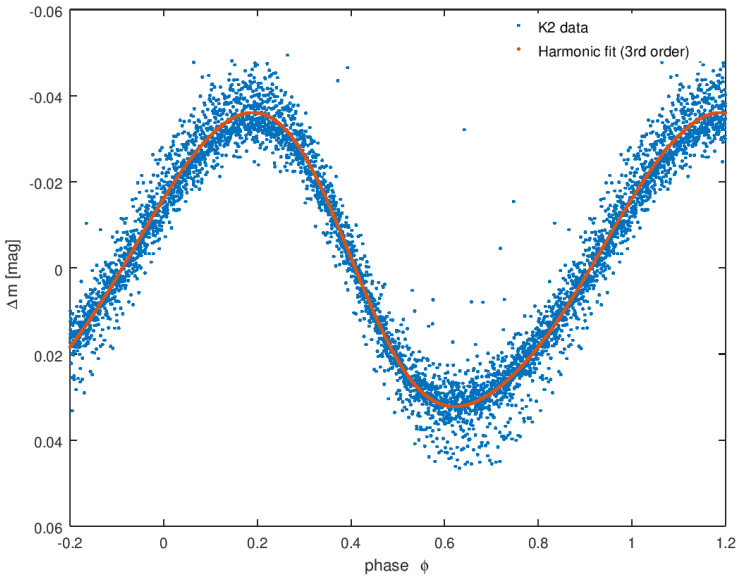

Figure 4.5: Comparison of observed and fitted data of white dwarf with EPIC 220171396.

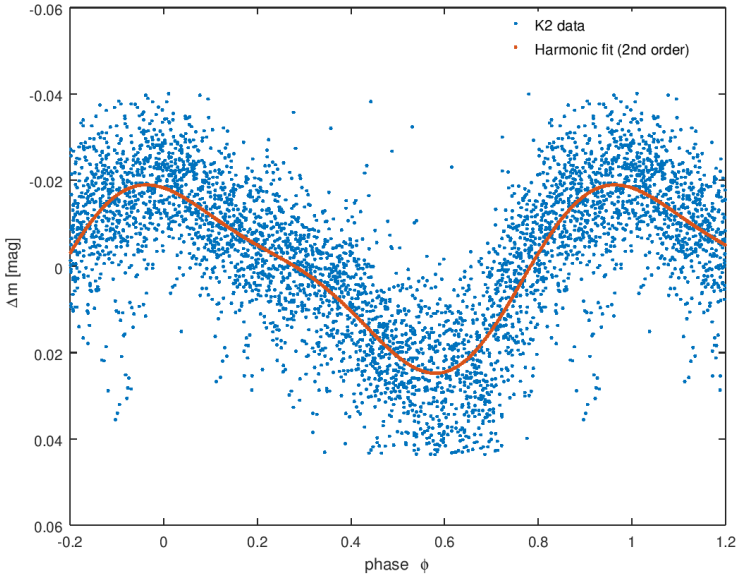

Figure 4.6: Comparison of observed and fitted data of white dwarf with EPIC 211815847.

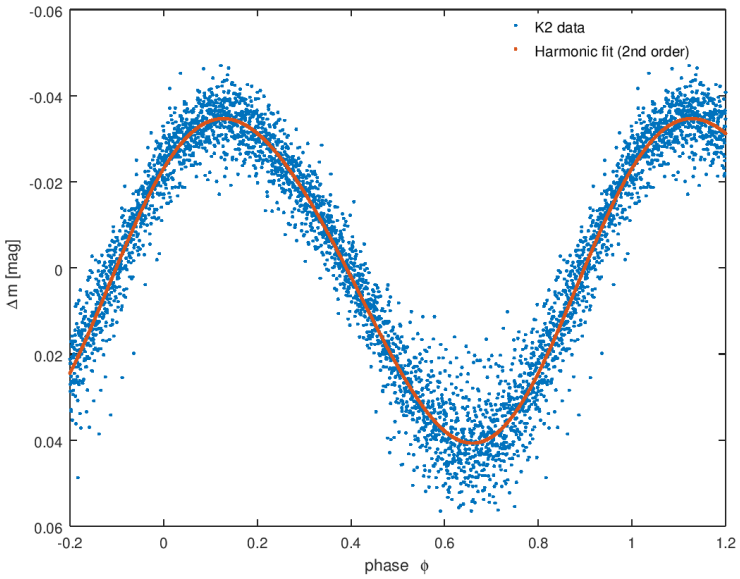

Figure 4.7: Comparison of observed and fitted data of white dwarf with EPIC 206197016.

5 Conclusion

Our goal in this work was to process light curves of white dwarfs from K2 mission of Kepler space telescope that are publicly available on Mikulski Archive for Space Telescopes and calculate the rotational periods of the white dwarfs showing variability.

We have carried out light curves and rotational periods for 33 white dwarfs observed by K2 mission which were picked out of approximatley 1600 white dwarfs. This only takes up about 2% of our starting number of white dwarfs. Our calculated periods range from about 10 hours up to 25 days.

Our results corresponds with recent papers that deal with rotating white dwarfs from K2 mission (de Lira et al., 2019) where their results varied from about a half a day to two dozens of days.

Electronic references

(E1) HR diagram of white dwarfs from GAIA satellite
http://sci.esa.int/science-e-media/img/31/ESA_Gaia_DR2_HRD_white_dwarfs.jpg
(E2) Cooling of white dwarfs with different masses and the effect of crystalization from GAIA satellite
http://sci.esa.int/science-e-media/img/76/ESA_Gaia_WhiteDwarfsHRD.jpg
(E3) Kepler objectives
https://keplerscience.arc.nasa.gov/objectives.html
(E4) Kepler space telescope
https://keplerscience.arc.nasa.gov/the-kepler-space-telescope.html
(E5) Kepler's second mission: K2
https://www.nasa.gov/mission_pages/kepler/overview/index.html
(E6) Kepler's second mission: K2
https://archive.stsci.edu/missions-and-data/k2
(E7) Kepler and K2 Observations of White Dwarf Stars
http://k2wd.org/
(E8) Mikulski Archive for Space Telescopes
https://archive.stsci.edu/

References

Barstow, M. A. et al. (2011). "White dwarfs in the UKIRT Infrared Deep Sky Survey Large Area Survey: the substellar companion fraction". In: *Monthly Notices of the Royal Astronomical Society*.

Briggs, G. P. et al. (2015). "Merging binary stars and the magnetic white dwarfs". In: *Monthly Notices of the Royal Astronomical Society*.

Charbonnel, C. and S. Talon (2005). "Influence of Gravity Waves on the Internal Rotation and Li Abundance of Solar-Type Stars". In: *Science*.

Christian, D. J. et al. (1997). "EUVE J0317 – 855: a rapidly rotating, high-field magnetic white dwarf". In: *Monthly Notices of the Royal Astronomical Society*.

de Lira, S R et al. (2019). "A wavelet analysis of photometric variability in Kepler white dwarf stars". In: *Monthly Notices of the Royal Astronomical Society*.

Fontaine, G., P. Brassard, and P. Bergeron (2001). "The Potential of White Dwarf Cosmochronology". In: *Publications of the Astronomical Society of the Pacific*.

Fulton, B. J. et al. (2014). "A search for planetary eclipses of white dwarfs in the Pan-STARRS1 medium-deep fields". In: *The Astrophysical Journal*.

García-Berro, Enrique et al. (2012). "Double degenerate mergers as progenitors of high-field magnetic white dwarfs". In: *The Astrophysical Journal*.

García-Segura, G. et al. (2014). "Single rotating stars and the formation of bipolar planetary nebula". In: *The Astrophysical Journal*.

Gänsicke, B. T. et al. (2011). "DA white dwarfs in Sloan Digital Sky Survey Data Release 7 and a search for infrared excess emission". In: *Monthly Notices of the Royal Astronomical Society*.

Heger, A. and N. Langer (1998). "The spin-up of contracting red supergiants". In: *Astronomy and Astrophysics*.

Heger, A. et al. (2003). "How Massive Single Stars End Their Life". In: *The Astrophysical Journal*.

Hermes, J. J. et al. (2017). "White Dwarf Rotation as a Function of Mass and a Dichotomy of Mode Line Widths: Kepler Observations of 27 Pulsating DA White Dwarfs through K2 Campaign 8". In: *The Astrophysical Journal Supplement Series*.

Iben Jr., I. and A. V. Tutukov (1984). "Supernovae of type I as end products of the evolution of binaries with components of moderate initial mass (M not greater than about 9 solar masses)". In: *The Astrophysical Journal*.

Isern, Jordi et al. (2017). "A Common Origin of Magnetism from Planets to White Dwarfs". In: *The Astrophysical Journal*.

Jura, M. (2003). "A Tidally Disrupted Asteroid around the White Dwarf G29-38". In: *The Astrophysical Journal*.

Jura, M. and E.D. Young (2014). "Extrasolar Cosmochemistry". In: *Annual Review of Earth and Planetary Sciences*.

Kawka, A. (2018). "The properties and origin of magnetic fields in white dwarfs". In: *Contributions of the Astronomical Observatory Skalnate Pleso*.

Kawka, A. and S. Vennes (2004). "Ap stars as progenitors of magnetic white dwarfs". In: *Proceedings of the International Astronomical Union*.

Kawka, A. et al. (2007). "Spectropolarimetric Survey of Hydrogen-rich White Dwarf Stars". In: *The Astrophysical Journal*.

Kepler, S. O. et al. (2007). "White dwarf mass distribution in the SDSS". In: *Monthly Notices of the Royal Astronomical Society*.

Kilic, Mukremin et al. (2006). "Debris Disks around White Dwarfs: The DAZ Connection". In: *The Astrophysical Journal*.

Koester, D. (2009). "Accretion and diffusion in white dwarfs - New diffusion timescales and applications to GD and G38". In: *Astronomy and Astrophysics*.

Koester, D. and G. Chanmugam (1990). "Physics of white dwarf stars". In: *Reports on Progress in Physics*.

Koester, D., B. T. Gänsicke, and J. Farihi (2014). "The frequency of planetary debris around young white dwarfs". In: *Astronomy and Astrophysics*.

Koester, D. and D. Wilken (2006). "The accretion-diffusion scenario for metals in cool white dwarfs". In: *Astronomy and Astrophysics*.

Krtička, J. et al. (2018). "Light variability of white dwarfs and subdwarfs due to surface abundance spots". In: *21st European Workshop on White Dwarfs* [in print].

Külebi, B. et al. (2009). "Analysis of hydrogen-rich magnetic white dwarfs detected in the Sloan Digital Sky Survey*". In: *Astronomy and Astrophysics*.

Kvasnica, Jozef (1998). *Statistická fyzika*. Praha: Academia.

Landolt, Arlo U. (1968). "A New Short-Period Blue Variable". In: *Astrophysical Journal*.

Laughlin, G., P. Bodenheimer, and F. C. Adams (1997). "The End of the Main Sequence". In: *The Astrophysical Journal*.

Liebert, James, P. Bergeron, and J. B. Holberg (2003). "The True Incidence of Magnetism Among Field White Dwarfs". In: *The Astronomical Journal*.

Luyten, W. J. (1949). "An Atlas of Identification Charts of White Dwarfs." In: *The Astrophysical Journal*.

Manser, Christopher J. et al. (2015). "Doppler imaging of the planetary debris disc at the white dwarf SDSS J122859.93+104032.9". In: *Monthly Notices of the Royal Astronomical Society*.

Maoz, Dan and Na'ama Hallakoun (2017). "The binary fraction, separation distribution and merger rate of white dwarfs from SPY". In: *Monthly Notices of the Royal Astronomical Society*.

Maoz, Dan, Na'ama Hallakoun, and Carles Badenes (2018). "The separation distribution and merger rate of double white dwarfs: improved constraints". In:

Martin, B. and D. T. Wickramasinghe (1986). "Magnetic blanketing in white dwarfs". In: *Monthly Notices of the Royal Astronomical Society*.

Martin, Brian and D. T. Wickramasinghe (1979). "Cyclotron absorption in magnetic white dwarfs". In: *Monthly Notices of the Royal Astronomical Society*.

Mikulášek, Z. and J. Krtička (2015). *Fyzika horkých hvězd*. `https://astro.physics.muni.cz/download/documents/skripta/F7601_2.pdf`.

Mikulášek, Z. and M. Zejda (2013). *Proměnné hvězdy*. `https://astro.physics.muni.cz/download/documents/skripta/F5540.pdf`.

Mikulášek, Z. and J. Krtička (2005). *Úvod do fyziky hvězd*. `https://astro.physics.muni.cz/download/documents/skripta/F3080.pdf`.

Murdin, P (2001). *Encyclopedia of Astronomy and Astrophysics*. IOP Publishing/Nature Publishing Group.

Nomoto, K. (1984). "Evolution of 8 - 10 solar mass stars toward electron capture supernovae. I - Formation of electron-degenerate O + Ne + Mg cores". In: *The Astrophysical Journal*.

Nomoto, K. and Y. Kondo (1991). "Conditions for accretion-induced collapse of white dwarfs". In: *The Astrophysical Journal Letters*.

Nordhaus, J. et al. (2011). "Formation of high-field magnetic white dwarfs from common envelopes". In: *Proceedings of the National Academy of Science*.

Potter, Adrian T. and Christopher A. Tout (2010). "Magnetic field evolution of white dwarfs in strongly interacting binary star systems". In: *Monthly Notices of the Royal Astronomical Society*.

Schmidt, Gary D. et al. (2003). "Magnetic White Dwarfs from the Sloan Digital Sky Survey: The First Data Release". In: *The Astrophysical Journal*.

Shipman, H. L. (1979). "Masses and radii of white-dwarf stars. III - Results for 110 hydrogen-rich and 28 helium-rich stars". In: *The Astrophysical Journal*.

Spruit, H. C. (2002). "Dynamo action by differential rotation in a stably stratified stellar interior". In: *Astronomy and Astrophysics*.

Suijs, M. P. L. et al. (2008). "White dwarf spins from low-mass stellar evolution models". In: *Astronomy and Astrophysics*.

Tout, C. A. et al. (2008). "Binary star origin of high field magnetic white dwarfs". In: *Monthly Notices of the Royal Astronomical Society*.

Tremblay, P.-E. et al. (2015). "On The Evolution of Magnetic White Dwarfs". In: *The Astrophysical Journal*.

Tremblay, Pier-Emmanuel et al. (2019). "Core crystallization and pile-up in the cooling sequence of evolving white dwarfs". In: *Nature*.

Webbink, R. F. (1984). "Double white dwarfs as progenitors of R Coronae Borealis stars and Type I supernovae". In: *The Astrophysical Journal*.

Wickramasinghe, D. T. and Lilia Ferrario (2005). "The origin of the magnetic fields in white dwarfs". In: *Monthly Notices of the Royal Astronomical Society*.

Wickramasinghe, Dayal T., Christopher A. Tout, and Lilia Ferrario (2013). "The most magnetic stars". In: *Monthly Notices of the Royal Astronomical Society*.

Woosley, S. E., A. Heger, and T. A. Weaver (2002). "The evolution and explosion of massive stars". In: *Rev. Mod. Phys.*

Zucker, Shay, Tsevi Mazeh, and Tal Alexander (2007). "Beaming Binaries: A New Observational Category of Photometric Binary Stars". In: *The Astrophysical Journal*.

Zuckerman, B. et al. (2003). "Metal Lines in DA White Dwarfs". In: *The Astrophysical Journal*.

Zuckerman, B. et al. (2010). "Ancient Planetary Systems are Orbiting a Large Fraction of White Dwarf Stars". In: *The Astrophysical Journal*.

Appendices

A Light curves of white dwarfs

Below is shown the rest of our light curves of white dwarfs fitted with proper orders of harmonic function.

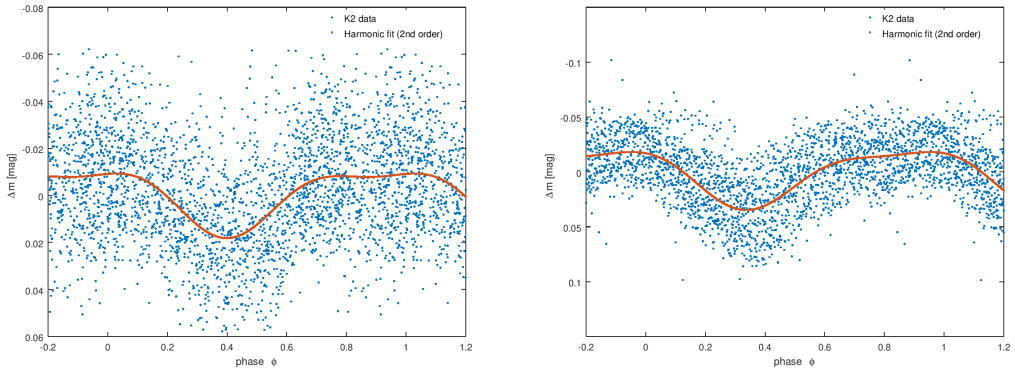

Figure A.1: Comparison of observed and fitted data of white dwarfs EPIC 201287505 (left), EPIC 201292141 (right).

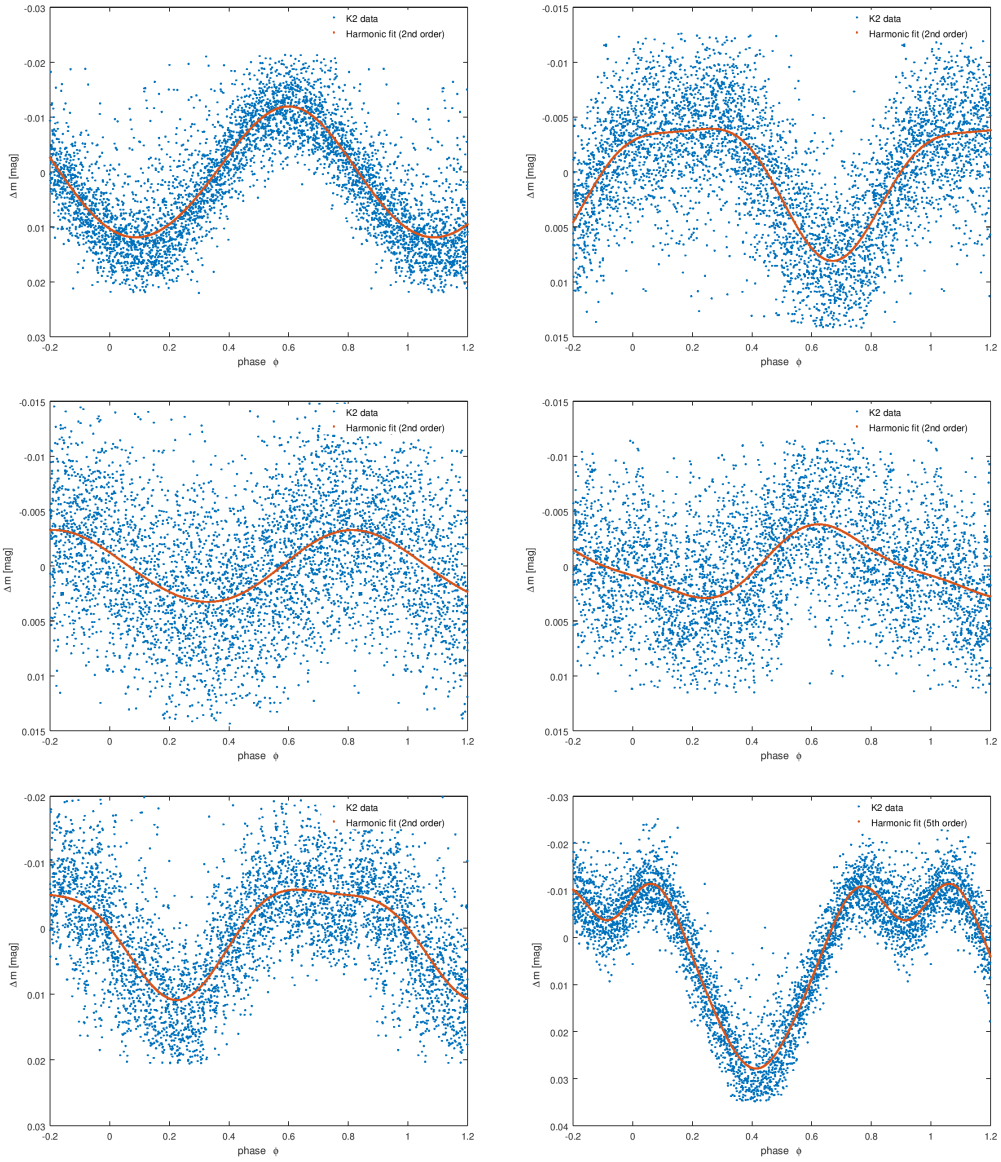

Figure A.2: Comparison of observed and fitted data of white dwarfs EPIC 201391671 (left top), EPIC 201475790 (right top), EPIC 201540753 (left middle), EPIC 206093851 (right middle), EPIC 206293521 (left bottom), EPIC 210609259 (right bottom).

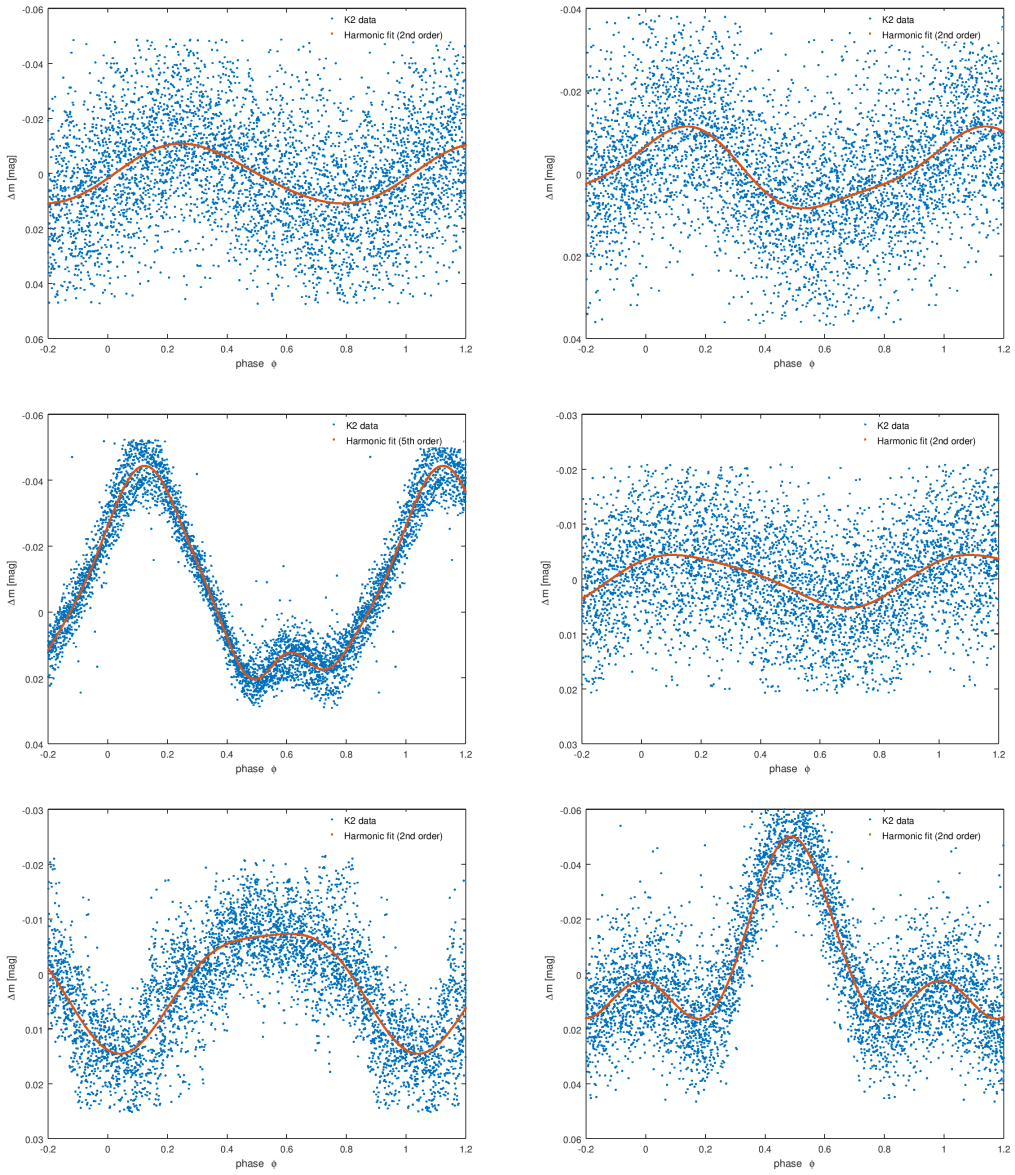

Figure A.3: Comparison of observed and fitted data of white dwarfs EPIC 211375959 (left top), EPIC 211434324 (right top), EPIC 211481191 (left middle), EPIC 211719633 (right middle), EPIC 211949591 (left bottom), EPIC 211995459 (right bottom).

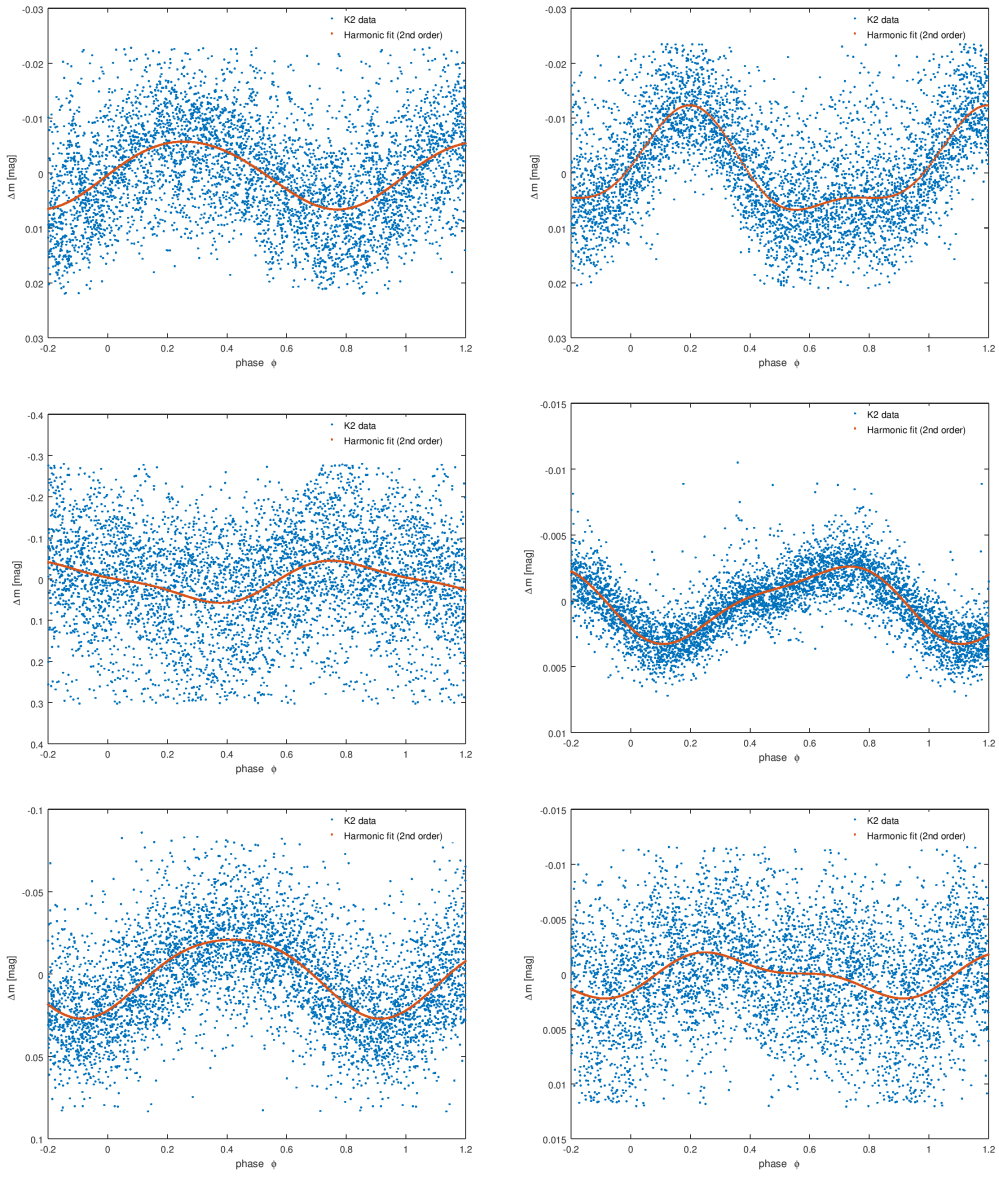

Figure A.4: Comparison of observed and fitted data of white dwarfs EPIC 220155299 (left top), EPIC 220178204 (right top), EPIC 220512358 (left middle), EPIC 220697132 (right middle), EPIC 228682372 (left bottom), EPIC 228682397 (right bottom).

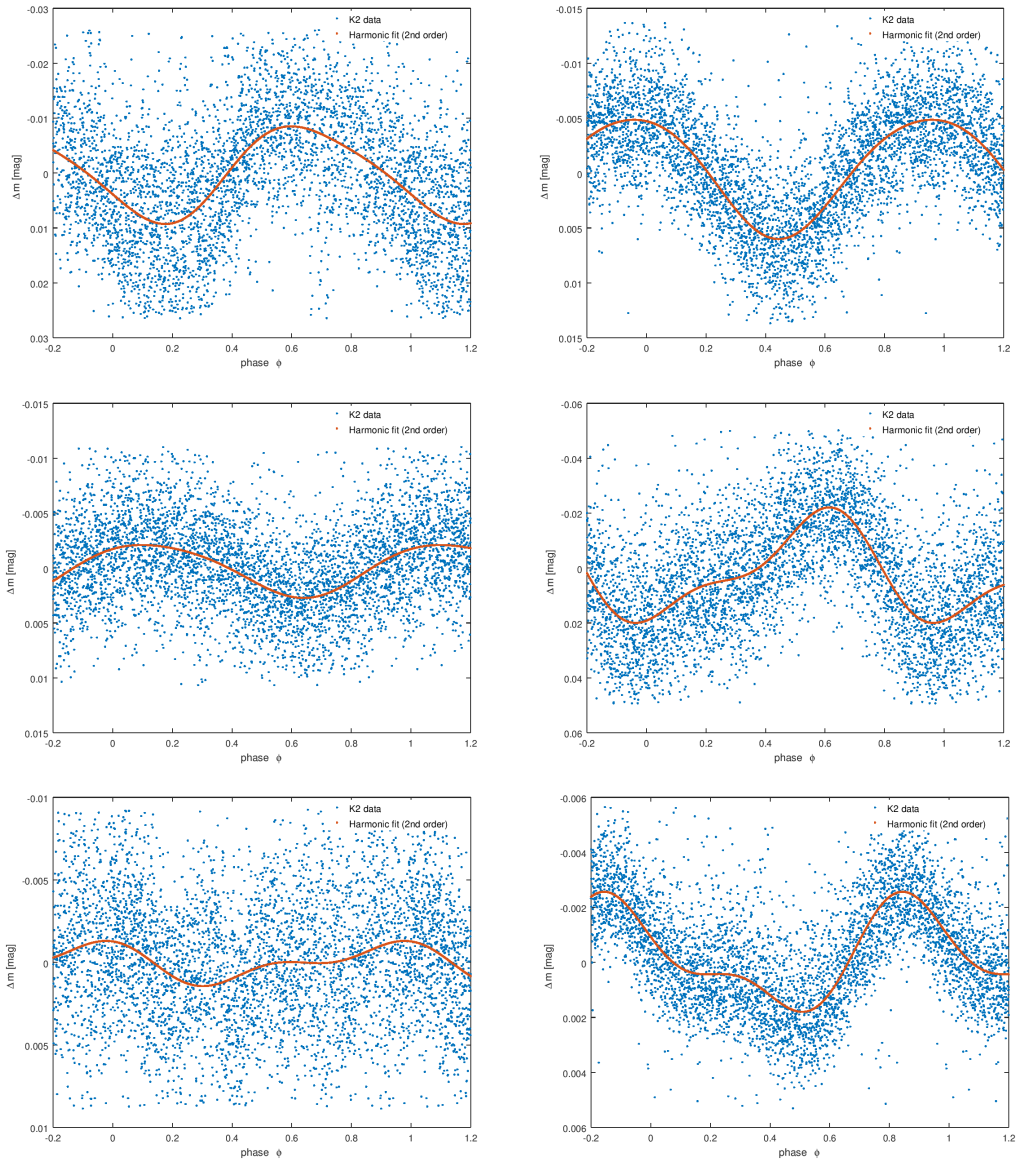

Figure A.5: Comparison of observed and fitted data of white dwarfs EPIC 246032223 (left top), EPIC 248460642 (right top), EPIC 248473806 (left middle), EPIC 248563865 (right middle), EPIC 248750313 (left bottom), EPIC 248774401 (right bottom).

B Atypical light curves of white dwarfs

Here we put several light curves with unusuall development where most of them are original light curves from Kepler Space Telescope.

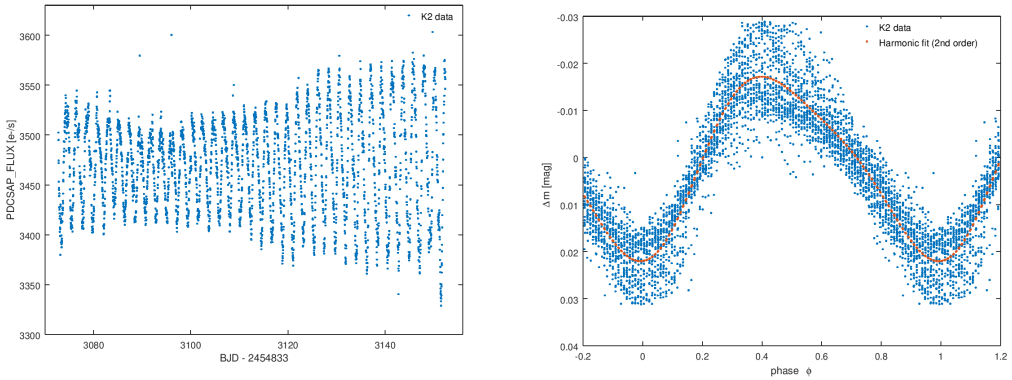

Figure B.1: The original data of white dwarf EPIC 248596522 with variable amplitude and our light curve with fitted function.

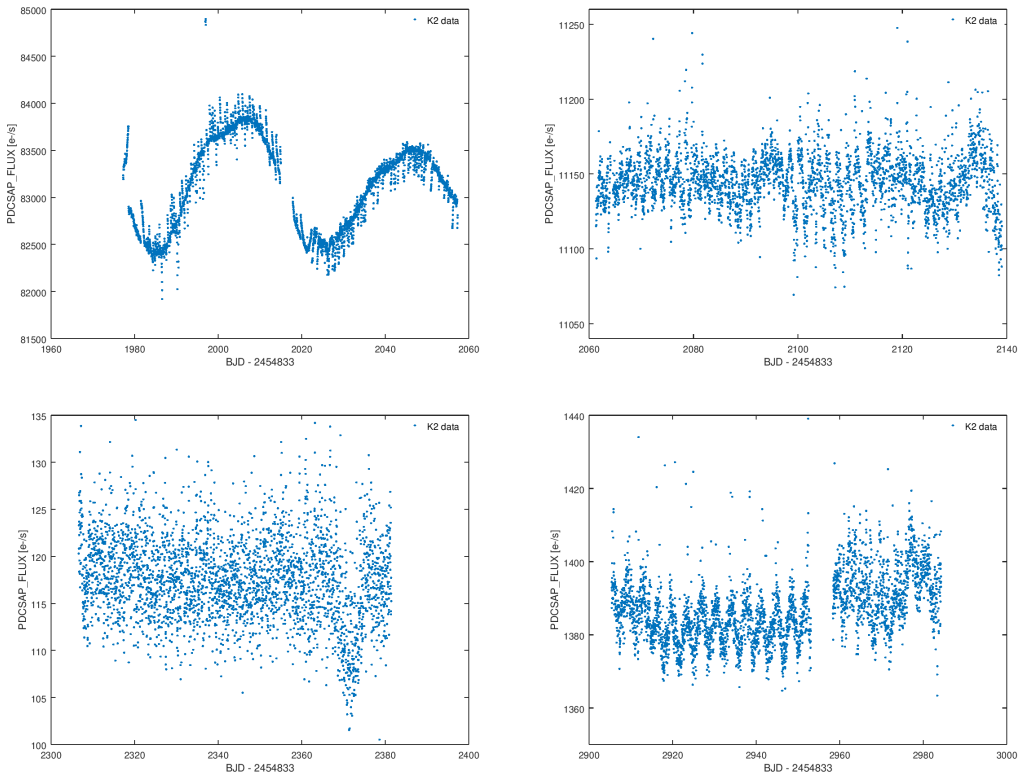

Figure B.2: The original data of white dwarfs EPIC 201932945 (top left), EPIC 203705962 (top right), EPIC 211908265 (bottom left) and EPIC 246083909 (bottom right).

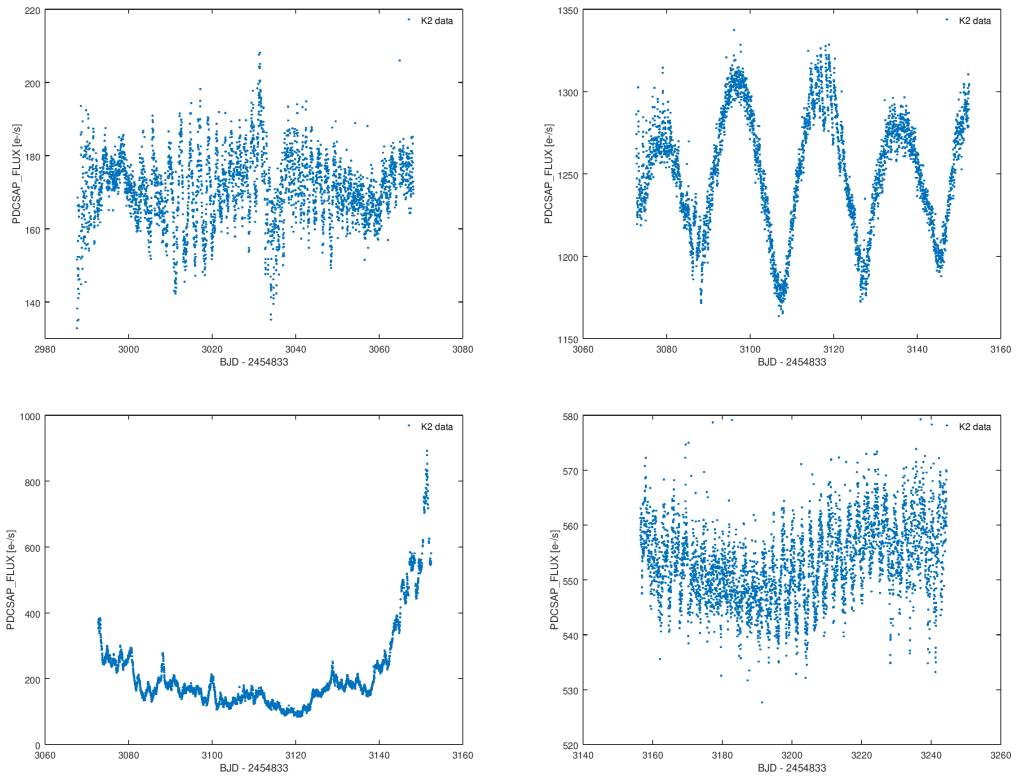

Figure B.3: The original data of white dwarfs EPIC 247710612 (top left), EPIC 248519839 (top right), EPIC 248616493 (bottom left) and EPIC 249579776 (bottom right).